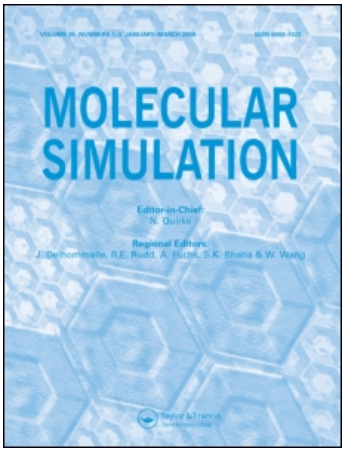

Molecular Simulation
Publication details, including instructions for authors and subscription information:
http://www.informaworld.com/smpp/title~content=t713644482

Optical and Computational Studies of Elastic and Defect Properties of Materials

J. D. Comins[a]
[a] Department of Physics and Condensed Matter Physics Research Unit, University of the Witwatersrand, WITS, South Africa

To cite this Article Comins, J. D.(1998) 'Optical and Computational Studies of Elastic and Defect Properties of Materials', Molecular Simulation, 21: 2, 67 — 87
To link to this Article: DOI: 10.1080/08927029808022052
URL: http://dx.doi.org/10.1080/08927029808022052

Molecular Simulation, 1998, Vol. 21, pp. 67–87
Reprints available directly from the publisher
Photocopying permitted by license only

OPTICAL AND COMPUTATIONAL STUDIES OF ELASTIC AND DEFECT PROPERTIES OF MATERIALS

J. D. COMINS

Department of Physics and Condensed Matter Physics Research Unit, University of the Witwatersrand, Johannesburg, Private Bag 3, WITS 2050, South Africa

(Received January 1998; accepted January 1998)

Experimental studies on a variety of different systems by means of optical spectroscopic methods are described together with appropriate computational approaches to model their behaviour. Investigations are described of superionic compounds by Brillouin scattering, of opaque solids and thin supported films by surface Brillouin scattering, and of halogen clusters in irradiated alkali halides by Raman scattering and optical absorption.

Keywords: Light scattering; superionic; thin film; elasticity; radiolysis; defect

INTRODUCTION

Optical spectroscopic techniques provide a powerful means of investigating the structural, vibrational, elastic, and defect properties of solid-state materials. Light, being a contact-free probe, allows non-destructive measurements on materials which can be made under extreme conditions of high and low temperatures and/or high pressures. In the interpretation and understanding of the results of these types of experiments, computational modelling techniques are playing an increasingly important role. Conversely, measurements of elastic properties provide essential data for the determination of interatomic potentials used in computer simulation codes [1].

In this paper, the results of a number of different optical spectroscopic experiments on a variety of materials are described together with appropriate

computational approaches. These include Brillouin scattering studies on superionic crystals, surface Brillouin scattering investigations on opaque solids and thin films, and Raman and optical absorption studies of irradiation-induced defects in alkali halides.

OPTICAL AND COMPUTATIONAL STUDIES

Brillouin Scattering in Superionic Conductors

There are a number of ionic compounds which display anomalously high ionic conductivity in the solid state; in cases where the conductivity is comparable to that of ionic melts, they are known as superionic, or fast-ion conductors [2–5]. These compounds are of technological importance and of fundamental interest as a form of disordered solid whose properties, in some ways, are intermediate between normal solids and liquids.

Theoretical methods [1] such as molecular dynamics, Monte-Carlo approaches, computational lattice and defect simulations combined with a variety of experimental investigations [2–5] including ionic conductivity, specific heat, nuclear magnetic resonance, neutron scattering and light scattering have together resulted in the present level of understanding of these compounds.

One model of the development of the superionic state is the progressive thermally-induced disordering of a sublattice [2, 5]. The transition is associated with a specific heat anomaly, a substantial increase in ionic conductivity and, in the context of the current discussion, elastic anomalies which can be conveniently studied by means of Brillouin scattering. The simplest compounds which display these combined features have the fluorite or anti-fluorite structure. A considerable amount of work has been carried out on the alkaline-earth fluorides which have the fluorite structure, such as CaF_2 and its analogues, [5, 6] and some on Li_2S, an anti-fluorite compound [7]. More recently, studies have been made on the trigonal tysonite structured fluorides such as LaF_3, CeF_3 and NdF_3 [8–11]. A comprehensive account of the theory and practice of Brillouin scattering in superionic conductors appears in Comins *et al.* [12].

In Brillouin scattering from transparent crystals, bulk acoustic phonons modulate the permittivity and as a result of elastio-optic coupling lead to inelastic scattering of light. The resulting Brillouin components in the spectrum are symmetrically displaced in frequency in the range 0–100 GHz from the elastically scattered light. The details of the selection rules, which

depend on the polarization of the incident and scattered light and the form of the Brillouin tensors for the particular acoustic mode are given in some detail in the literature (see *e.g.*, Ref. [12] and references therein). The frequency shift of the scattered light is related directly to the mode velocity and in turn to the three eigenvalues γ of the Christoffel secular equation. The combination of elastic constants expressed in Voigt notation as C_{ij} constituting the eigenvalues γ are simplest for high-symmetry directions. In a limited number of cases, γ for a particular mode is related to a single elastic constant, but in general may be a relatively complicated combination of these. In order to determine a complete set of elastic constants for a crystal of a particular symmetry, Brillouin scattering measurements are required for a number of phonon propagation directions. Instrumentally, Brillouin scattering in solids is demanding [12]. The Brillouin scatterered components are many orders of magnitude weaker than the elastically scattered light and the frequency shifts are small. A multipass Fabry-Pérot interferometer using a stabilized laser source provides the necessary resolution and contrast. For transparent materials a triple-pass interferometer is adequate. High temperature measurements of fluoride compounds in the superionic region normally require the samples to be protected from contamination from oxygen and water vapour. Special encapsulation techniques have been developed for this purpose in which the oriented, cut and polished crystal specimens are sealed in silica capsules under ultra-pure low pressure argon gas. The measurements are conducted using a specially designed optical furnace to incorporate the silica capsules arranged for a 90° light-scattering geometry.

Phenomenological models developed to account for the diffuse transition to the superionic state have been based on defect interactions [6, 12–15]. Such models are discussed in terms of the free energy of the crystal:

$$F(n) = nh_0 - h_i(n) - nS_vT - S_c(n)T \tag{1}$$

where n is the Frenkel defect concentration, h_0 is the Frenkel defect formation energy at $n = 0$, $h_i(n)$ is the defect interaction energy which reduces the effective formation energy as n increases, S_v is the defect vibrational entropy and S_c is the configurational entropy. This model is qualitatively successful in accounting for the diffuse transition in terms of an increase in Frenkel defect concentration on a particular sublattice which rises rapidly near the transition temperature T_c as a result of attractive defect interactions. At relatively large defect concentrations $n \geq 0.1$, repulsive interactions suppress the further generation of defects.

In the case of computer simulations and their relation to the Brillouin scattering experiments to be described, the most relevant are lattice energy calculations which enable the elastic constants to be determined. The effect of defects can be advantageously incorporated by supercell procedures. Pair interactions between ions are described by the appropriate potential functions and the ionic polarizability is included using the shell model. Elastic constants are defined as the second derivatives of the lattice energy with respect to strain, with the lattice energy normalised to unit volume. The details of the computational techniques are given in detail by Catlow and Mackrodt [16] and summarised in Comins *et al.* [12]. The principles are incorporated within the computational routines PLUTO and THBREL.

As an illustration of a successful Brillouin scattering and computational study, we shall consider the work of Ngoepe *et al.* [9] on LaF_3. Figure 1 shows the structure of LaF_3 which is representative of the tysonite structured fluorides. As shown, both trigonal and hexagonal space groups have been suggested for this structure; in practice the hexagonal structure is an adequate description for the Brillouin scattering results.

Brillouin scattering experiments performed at high temperatures and for a sufficiently large number of phonon propagation directions resulted in a set of elastic constants as a function of temperature. The results are shown in Figure 2. The initial linear decrease in the elastic constants is associated with normal lattice anharmonicity leading to thermal expansion. Above a transition temperature (T_c) of 1150 K there are pronounced changes in the elastic constants which correspond to an anomalous increase in the specific heat capacity [17].

Relevant computational simulations include those by Jordan and Catlow [18] who used the CASCADE code to resolve the controversy about the relative mobilities of fluorine ions on the different sublattices and calculated the formation energies of Schottky and anion Frenkel defects. Although Schottky disorder had been indicated by lattice parameter and dilation studies below 1000 K, [19] their calculations favour anion Frenkel disorder on energetic grounds.

Computer simulations by Ngoepe *et al.* [9] using a defect supercell approach in conjuction with the THBREL program determined the lattice energies and the elastic constants in LaF_3 which were compared with the Brillouin scattering results in Figure 2. The linear reductions in the elastic constants below T_c were well reproduced as shown in Table I, by appropriately enlarging the lattice according to the experimentally measured expansion. The crucial aspect of the thermodynamic model of the diffuse transition, namely an increasing defect interaction energy as the defect

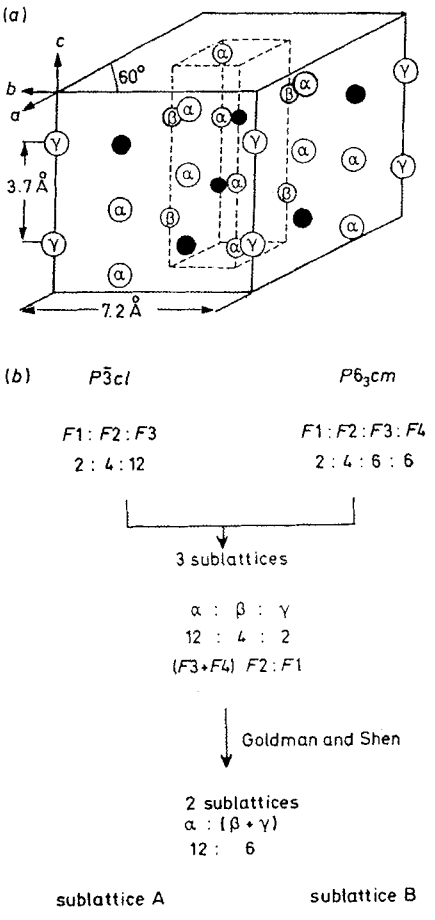

FIGURE 1 (a) Fluorine sublattice models in LaF_3. The diagram shows a simplified structure of LaF_3. Fluorine sublattice A consists of α-sites and sublattice B consists of β- and γ-sites. • indicates the La^{3+} sites; (b) Shows proposed models of LaF_3 (after Ngoepe *et al.* [9]).

concentration increases (Eq. 1) is reproduced by the calculations (Tab. II). Table III shows the calculated fractional changes in the elastic constants in addition to the linear decreases due to anharmonicity. Both anion Frenkel and Schottky disorder result in the reduction of most of the elastic constants. However there is much better agreement in the behaviour of C_{44} with the assumption of Frenkel disorder rather than Schottky defects. An overall concentration of 2 mol% of anion Frenkel defects provides a satisfactory explanation of the experimental results.

Although the above work appears self-consistent in relation to LaF_3, studies of CeF_3 [10] and NdF_3 [11] while showing essentially similar

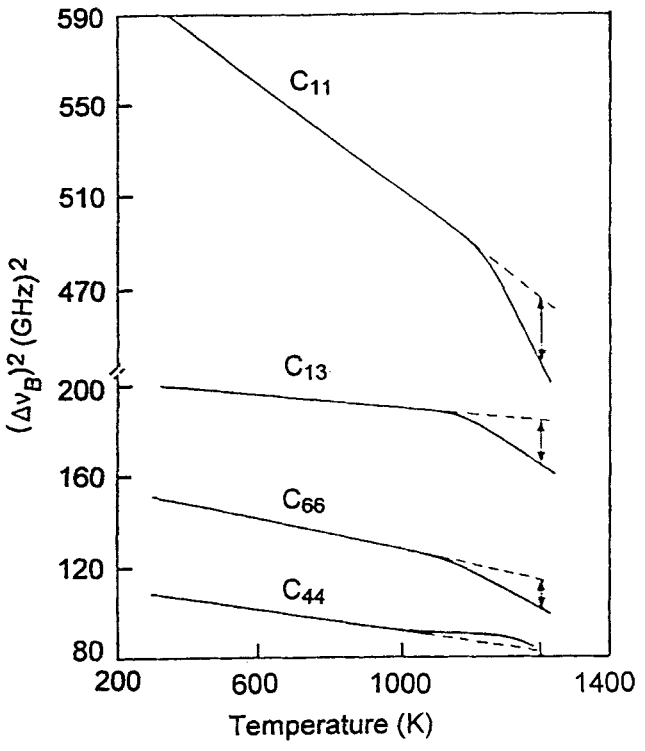

FIGURE 2 Temperature dependence of the square of the Brillouin scattering frequencies $(\Delta\nu_B)^2$corresponding to various elastic in LaF_3. The results are calculated from measured acoustic-mode frequencies in several propagation directions (after Ngoepe *et al.* [9]).

TABLE I Comparison of the calculated and experimental temperature gradients dC_{ij}/dT of the various elastic constants of LaF_3 below 1150 K (after Ngoepe *et al.* [9])

C_{ij}	dC_{ij}/dT	
	Experimental MPa/K	*Calculated MPa/K*
C_{11}	34.4	37.2
C_{33}	48.8	34.8
C_{13}	5.4	7.6
C_{66}	10.4	13.0
C_{44}	6.7	7.6

behaviour as regards the elastic constants as measured by Brillouin spectroscopy, have significantly different variations of the specific heat capacity as shown in Figure 3. The specific heat anomalies for CeF_3 [20] and NdF_3 [21] are similar, but have a smaller magnitude and a different functional form to that of LaF_3 [17]. The reasons for these differences are not

TABLE II Energies associated with defect supercells in LaF_3. Asterisk denotes zero-value result from recombination during energy minimisation (after Ngoepe *et al.* [9])

		Frenkel model		*Schottky model*	
Supercell size unit cells	*Perfect lattice energy eV*	*Defect concentration %*	*Defect interaction energy eV*	*Defect concentration %*	*Defect interaction energy eV*
1	−293.05	5.56	0*	16.60	
2	−586.10	2.78	0.70	8.30	
3	−879.15	1.85	0.49	5.56	
4	−1172.20	1.39	0.44	4.17	2.92
6	−1758.30	0.93	0.35	2.78	2.60
8	−2344.40	0.47	–	2.09	–

Frenkel pair defect formation energy 2.27 eV.
Schottky quartet defect formation energy 5.64 eV.
*Zero value results from recombination during energy minimisation.

TABLE III Comparison of the experimental percentage deviations of the elastic constants from the extrapolated anharmonic values at 1400 K with those calculated on the basis of anion Frenkel and Schottky models (after Ngoepe *et al.* [9])

	Experimental 1400 *K*	*Frenkel model* 2 *mol%*	*Schottky model* 2 *mol%*
$\Delta C_{11}/C_{11}$	3.7	6.9	8.4
$\Delta C_{33}/C_{33}$	4.4	4.4	8.0
$\Delta C_{13}/C_{13}$	10.2	10.1	11.7
$\Delta C_{66}/C_{66}$	11.0	11.1	12.0
$\Delta C_{44}/C_{44}$	0.0	−3.0	15.8

obvious and computational simulations would be valuable in developing an explanation of these effects.

Surface Brillouin Scattering in Opaque Materials

Surface Brillouin scattering (SBS) has emerged in recent years as a valuable technique in the studies of surface acoustic excitations of opaque solids and thin supported layers [22–25].

In these cases, the surface ripple mechanism, rather than elastic-optic coupling is dominant. For thin layers, the combination of the substrate and overlayer determines the types of observed acoustic excitations localised near the surface. The frequency spectrum of the scattered light is a signature of the resulting surface dynamics and of the near-surface elastic properties of the materials which have an influence on these dynamics.

Theoretical and computational approaches using surface Green's functions [26–28] provide a comprehensive understanding of these sometimes

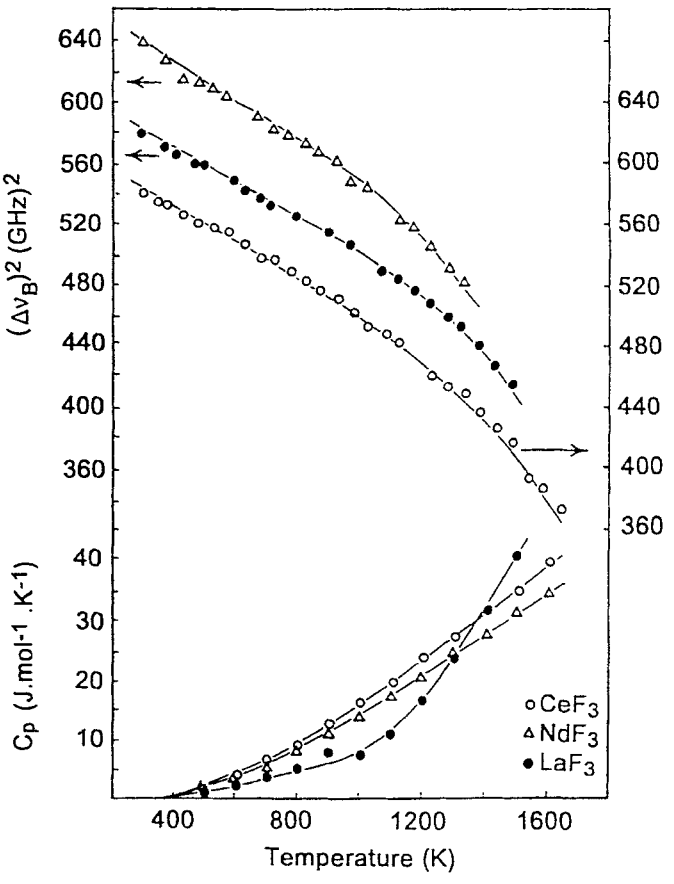

FIGURE 3 Temperature dependence of the square of the Brillouin scattering frequencies $(\Delta\nu_B)^2$ corresponding to elastic constant C_{11} for LaF_3, CeF_3 and NdF_3 (after Mjwara *et al.* [11]). Temperature dependence of ΔC_p, the difference between the experimental and Debye heat capacities for LaF_3, [17] CeF_3 [20] and NdF_3 [21].

complex and often weakly-scattering excitations. A typical backscattering geometry for SBS is shown in Figure 4. The wavevector **k** of the incident laser light makes an angle θ with the surface normal, and the spectrum of the light backscattered inelastically around $-\mathbf{k}$ is collected. Wavevector conservation applies only to the projection on the surface of the scattering wavevector. Hence, for backscattering, the surface modes which contribute to the light scattering are of wavevector $k_{\parallel} = 2k\sin\theta$. In the simplest case of an opaque isotropic solid, the scattering is usually dominated by an intense peak of angular frequency shift $\omega = vk_{\parallel}$ resulting from the Rayleigh surface acoustic wave (SAW) of velocity v. In addition, there is a considerably less

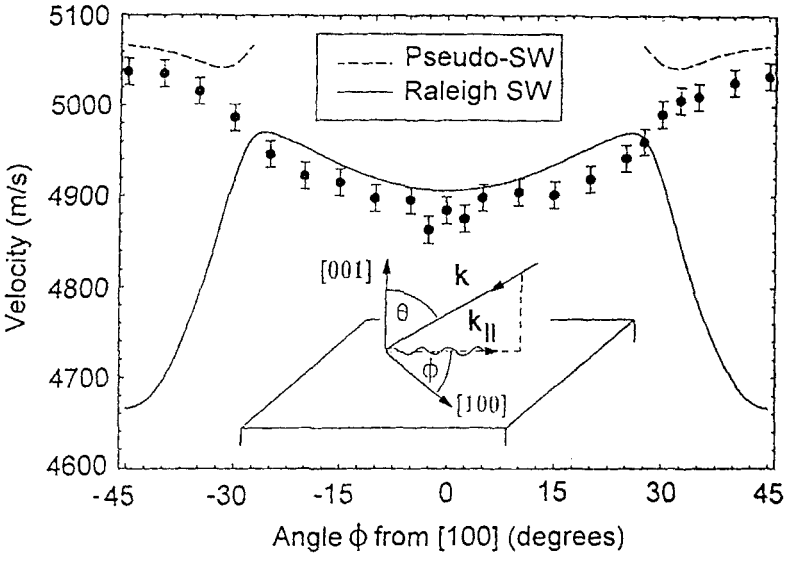

FIGURE 4 Brillouin scattering measurements of surface wave velocity on (001) *n*-type silicon at room temperature. The curves show the calculated SAW and pseudo-SAW velocities based on ultrasonic measurements of the elastic constants of silicon. The geometry of the back-scattering arrangement is illustrated in the insert (after Stoddart *et al.* [31]).

prominent "Lamb shoulder" extending to higher frequencies resulting from the coupling to the continuum of bulk modes by means of the displacements they cause at the surface. In the cases of anisotropic solids and thin films on substrates there are a great variety of structures found in the Brillouin spectra. The experimental requirements are considerably more demanding than those for Brillouin scattering from bulk excitations in transparent solids. The most commonly used instrument for the purpose is the Sandercock (3 + 3) tandem Fabry-Pérot interferometer with electronic stabilization and appropriate antivibration protection. A contrast of $\sim 10^{12}$ is attained which is sufficient for opaque materials.

At room temperature and above, the SBS efficiency for the surface ripple mechanism is proportional to

$$I(\omega) \alpha\ D \frac{T}{\omega} \mathrm{Im}\{\tilde{G}_{33}(\mathbf{k}_{\|}, \omega)\} \tag{2}$$

where T is the temperature. ω is the angular frequency shift, $\mathbf{k}_{\|}$ is the surface wavevector, $\tilde{G}_{33}(\mathbf{k}_{\|}, \omega)$ is the component of the Fourier (frequency and wavevector) domain elastodynamic Green's function pertaining to force

and response normal to the surface. The factor D depends on the medium (of permittivity $\in$ and density ρ), the incident photon frequency ω_0 and its polarization, and the scattering geometry.

As brief illustration of the theory, we consider the case of an overlayer on a substrate. The method takes into account the six phase-matched plane waves ($n = 1, 2, \ldots, 6$) in the overlayer and the three outgoing plane waves ($n = 7, 8, 9$) in the substrate as discussed, for example, in Farnell and Adler [29]. Using the boundary conditions for the surface tractions and displacements, nine equations are constructed for the partial wave amplitudes. The displacement Green's function $\tilde{G}_{33}(\mathbf{k}_\parallel, \Omega)$ is then represented by the superposition of the six partial waves in the film:

$$G_{33}(\mathbf{k}_\parallel, \omega) = \sum_{n=1}^{6} \frac{i}{\omega} (\mathbf{B}^{-1})_3^{(n)} U_3^{(n)} \exp(-ik_3^{(n)} h) \tag{3}$$

where $\mathbf{B}^{-1}$ is the boundary condition matrix, U_3 is the component of the mode polarization, k_3 is the wavevector component perpendicular to the free surface, and h is the overlayer thickness.

In SBS experiments, $\mathbf{k}_\parallel$ is determined by the experimental arrangement and scattering geometry and $G_{33}(\mathbf{k}_\parallel, \omega)$ and the Brillouin scattering intensity $I(\omega)$ depend on the spectral frequency shift ω. A true surface waves arises from the vanishing of $|\mathbf{B}|$, where $\mathbf{B}^{-1}$ becomes singular. This results in a sharp line in the spectrum, at a frequency smaller than the threshold bulk shear mode of the overlayer. Beyond a critical value of $k_\parallel h$ one or more pseudo-SAW's, corresponding to minima in $|\mathbf{B}|$ may exist in the bulk wave continuum or Lamb shoulder. These are surface modes which have a bulk wave component which results in energy radiating into the substrate and leads to their attenuation. A wealth of different types of excitations occur, depending on overlayer thickness and the relative magnitudes of the elastic constants of the overlayer and substrate. Appropriate modification of the theory presented above permits treatments of an anisotropic elastic half space, corresponding to the surface of a solid, or two elastic half spaces in contact, being relevant to interface modes.

As an initial example of SBS on opaque solids, we consider the work of Stoddart *et al.* [30, 31] in which the Brillouin spectrum was measured as a function of temperature and direction for the (001) surface of single crystal silicon. Figure 4 shows the scattering geometry, in which, by changing the angle ϕ while keeping angle θ fixed, the Brillouin spectrum was measured in the angular range extending out to 45° on either side of the [100] direction. In the range extending beyond 28° on either side of the [100] direction,

the spectrum is dominated by a pseudo-SAW. The SAW and pseudo-SAW velocities were measured as a functional of temperature to 800°C, and the elastic constants C_{11}, C_{12} and C_{44} determined by a least-squares fitting procedure. The results are shown in Figure 5. Careful correction of sources of systematic error produce results which are no more than 1% below ultrasonic values. This remaining discrepancy is probably due to effects such as surface roughness and surface damage caused by polishing.

Extensive SBS measurements have been carried out on TiN thin films on high speed steel (HSS) as a function of film thickness, temperature and stoichiometry/residual stress by Pang *et al.* [32] and Every *et al.* [33] Using the surface Green's function approach, calculated spectra for representative TiN film thicknesses are shown in Figure 6. For the thinnest film shown,

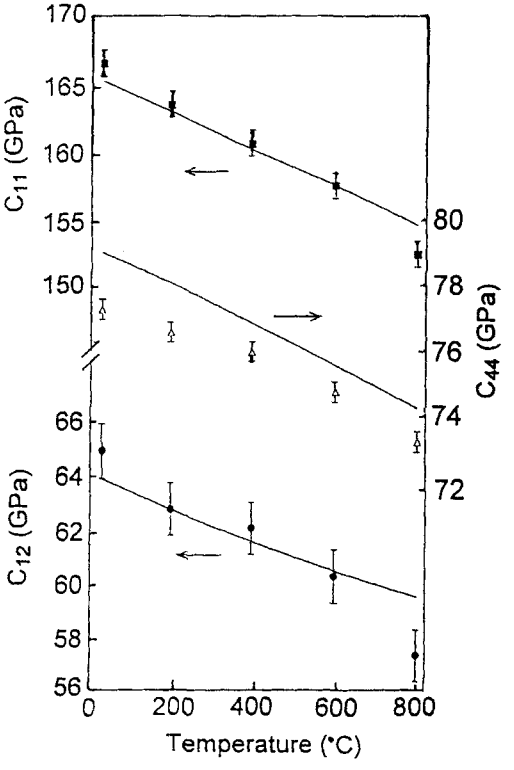

FIGURE 5 The three independent elastic constants of single crystal silicon have also been measured previously at high temperatures by ultrasonic methods. These results are compared here with the elastic constants found by least-squares minimization of the surface wave velocities. Note that the uncertainty in the ultrasonic measurements is not shown (after Stoddart *et al.* [31]).

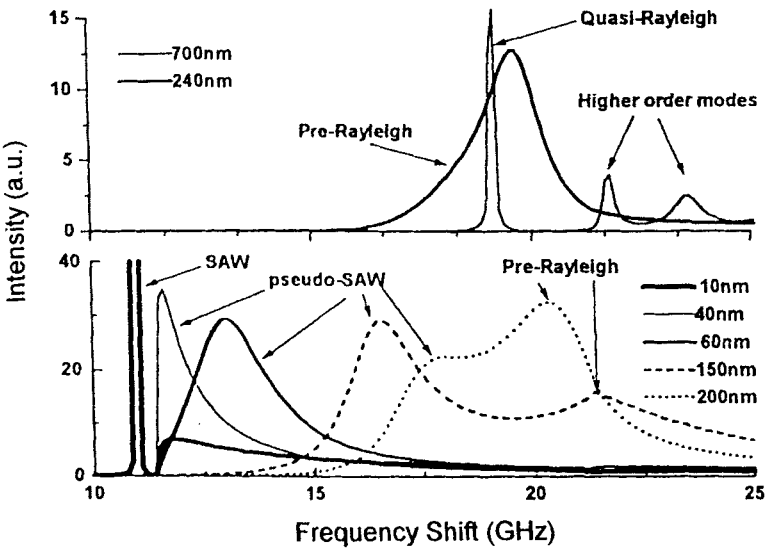

FIGURE 6 Calculated Brillouin spectra of TiN/HSS for a selection of film thickness h, displaying a true SAW, a highly damped pseudo-SAW, "pre-Rayleigh", quasi-Rayleigh and its higher order modes. In the calculations, $\mathbf{k}_{\|}$ is fixed by the back scattering geometry with the incident angle $\theta = 70°$. The scattering intensity is given in arbitrary units (after Every *et al.* [33]).

namely 10 nm, there is a sharp peak at 10.9 GHz which results from a true surface wave, together with the Lamb shoulder (bulk wave continuum) extending from the substrate transverse wave threshold (11.4 GHz) through the longitudinal wave threshold (21.3 GHz) to larger frequencies. For a film thickness of 40 nm the surface wave is merged into the Lamb shoulder. At 60 nm, a highly damped pseudo-SAW resulting in a broad band is evident. For 150 and 200 nm films a "pre-Rayleigh" mode emerges and rises to prominence followed by its evolution into the quasi-Rayleigh wave for film thicknesses of 700 nm and above. For the largest film thickness, higher order modes of greater frequency shifts and relatively lower intensity than the pseudo-SAW are observed.

Figure 7 shows the experimental Brillouin spectra for TiN/HSS for various film thicknesses ranging from 20 to 4180 nm. The results can be compared with those of Figure 6. For the bare HSS substrate, the Rayleigh wave is present, and as the film thickness increases up to 20 nm ($k_{\|}h = 0.46$), the peak in the Brillouin spectrum corresponds to a true SAW, but by 60 nm ($k_{\|}h = 1.37$) the peak has merged into the continuum and is a pseudo-SAW. For larger film thicknesses, the higher order modes of the quasi-Rayleigh

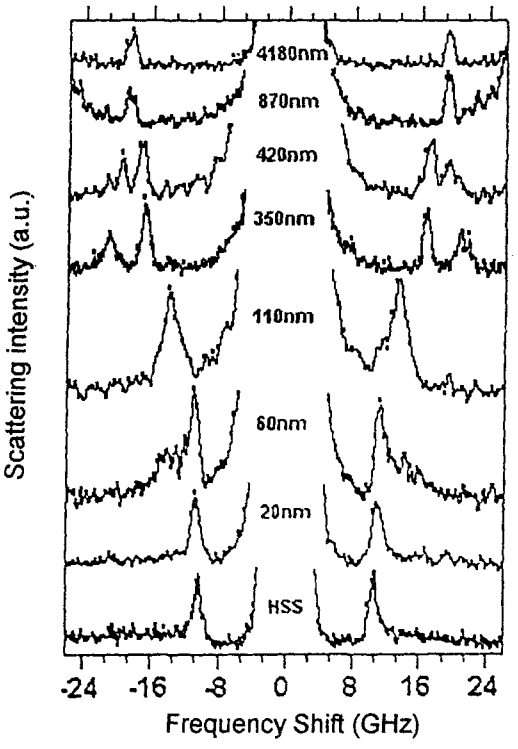

FIGURE 7 Experimental Brillouin spectra for TiN/HSS for various film thicknesses ranging from 20 to 4180 nm (after Every *et al.* [33]).

wave can be seen, *e.g.*, for the 350 nm ($k_{\|}h = 7.98$) and 420 nm ($k_{\|}h = 9.58$) films. Quasi-Rayleigh and several higher order modes are present for the 870 nm ($k_{\|}h = 19.84$) film, but for thick films *e.g.*, 4180 nm ($k_{\|}h = 95.34$) only the quasi-Rayleigh mode is resolved, since the higher order modes become too closely spaced to be observed. A comparison was made between the measured and calculated dispersion relations of surface wave velocity v *vs.* $k_{\|}h$. In this strongly stiffened situation, the elastic constants of TiN used in the calculations have a profound effect on the theoretical dispersion relation. Good agreement between the measured and calculated dispersion curves are obtained for reduced values of the elastic constants of TiN as shown in Figure 8. This effect is likely to be due to complex compositional variations at the TiN/HSS interface and involving oxides of titanium identified by XPS measurements which would significantly change the elastic and/or physical properties.

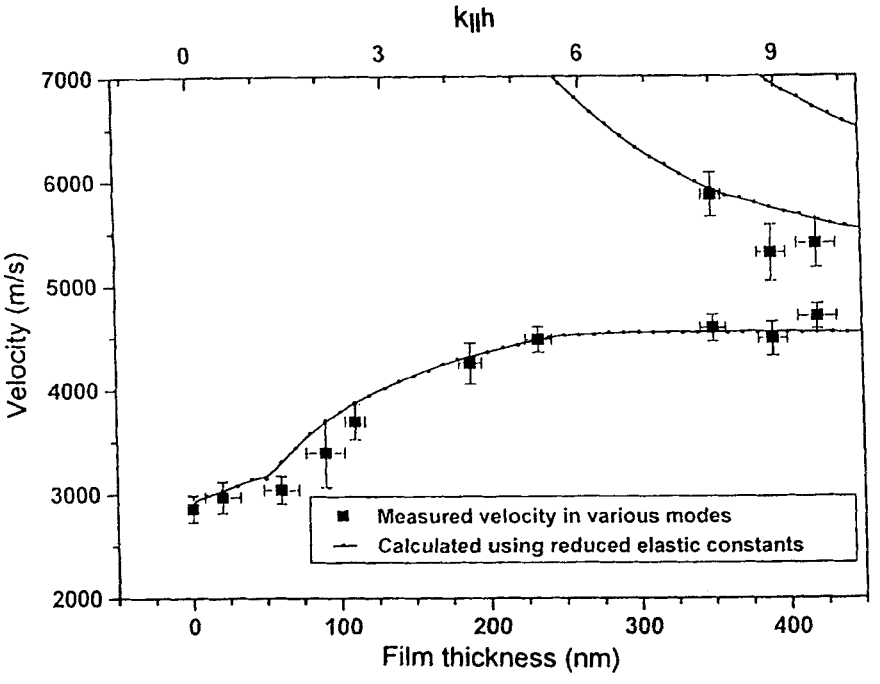

FIGURE 8 Comparison between the measured and calculated wave velocities of TiN/HSS as a function of film thickness (lower axis) and $\mathbf{k}_{\|}h$ (top axis), where the reduced elastic constants of TiN, which are 75% of the values for bulk TiN, are used in calculating the dispersion curves. (after Every *et al.* [33]).

Raman and Optical Absorption Studies of Irradiation-induced Defects in Alkali Halides

The combination of Raman and optical absorption measurements has in recent years provided new information concerning the structures of interstitial halogen defects formed during the exposure of alkali halide crystals to ionising radiation [34–42]. These halogen aggregates are inherently molecular in nature being formed from the so-called H-centres formed together wih F-centres in the primary excitonic mechanism of defect production [43, 44]. Computational simulations by Dienes *et al.* [45] and Catlow *et al.* [46] examined the stability and formation energies of associations of H-centres, which in isolated form become mobile at low temperatures, $\sim$40 K. Their work provided much stimulus to the field and the proposed structures considered by Catlow *et al.* [46] are shown in Figure 9. Their calculations using the HADES routine did not strongly distinguish

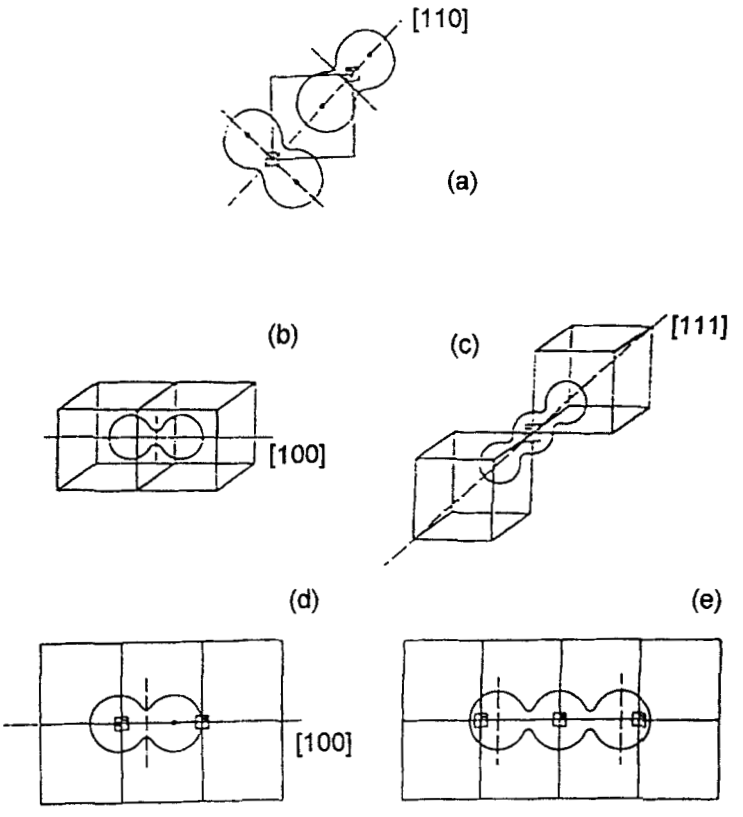

FIGURE 9 The possible configurations of the halogen di-interstitial. a) loosely bound di-*H*-centre; b) interstitial X_2 molecule; c) X_3^- molecular defect; d) molecule–vacancy pair complex; e) X_3^-- trivacancy complex. ⊞ : anion vacancy; ⊟ : cation vacancy (after Catlow *et al.* [46]).

between the various possible di-interstitial halogen configurations such as X_2^0 or X_3^- on energetic grounds. As a further possibility, the movement of anions and cations from their sites and the occupation of the resultant vacancy pairs by X_2^0 or X_3^- was shown to be energetically favourable; this exothermic reaction was postulated to result in the perfect dislocation loops observed by electron microscopy [47].

Raman and optical absorption studies by Allen and Comins [42] demonstrated the presence of I_3^- and I_n^- defects as majority aggregates of H-centres in RbI irradiated at 295 K, these having Raman transitions near 112 cm^{-1} and 172 cm^{-1} respectively, as well as a very weak Raman transition near 201 cm^{-1} which they associated with I_2^0. The Raman spectrum is shown in Figure 10. This clarified the long-standing controversy in regard to

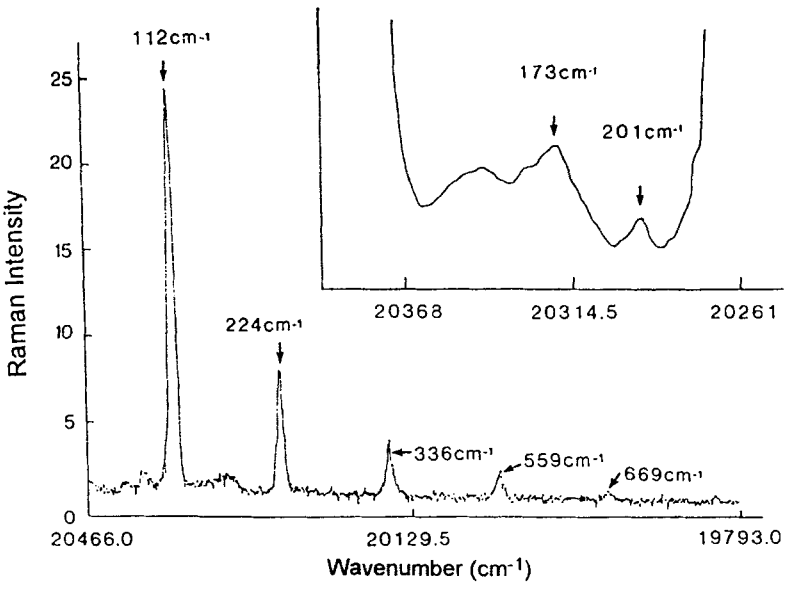

FIGURE 10 Raman spectrum obtained after γ-irradiation of RbI at 295 K to a dose of 250 Mrad. The main figure shows the 112 cm^{-1} fundamental and its overtones. The inset is plotted on expanded scales and shows the structure between the 112 cm^{-1} fundamental and its first overtone. The spectrum was measured at 80 K using a laser wavelength of 488 nm (after Allen and Comins [42]).

the dominent di-interstitial halogen defect, which is thus shown to be I_3^- for iodides. A similar result apparently holds for Br_3^- in alkali bromides [40]. In KI, on the other hand, while irradiations at low temperatures, *e.g.*, 200 K, result in I_3^- and I_n^- clusters, [34, 35] the dominant defects produced near room temperature are large $(I_2)_n$ aggregates, which at sufficiently high doses show the lattice modes of crystalline iodine, [37, 48] as shown in Figure 11.

There is now new and detailed information on the formation of halogen interstitial clusters in alkali iodides and a more limited number of studies on the bromides. In these cases, near resonance enhancement of the Raman transitions is possible with the excitation frequencies available with argon-ion lasers commonly used for Raman spectroscopy. Studies of the alkali chlorides in which the halogen interstitial clusters have optical absorption bands (V-bands) at higher frequencies will require laser excitation in the ultra-violet. In the context of computer simulations, it would be extremely valuable if the pioneering work of Catlow *et al.* [46] could be repeated and extended using more recently developed computational techniques and routines in order to accommodate the considerable body of new

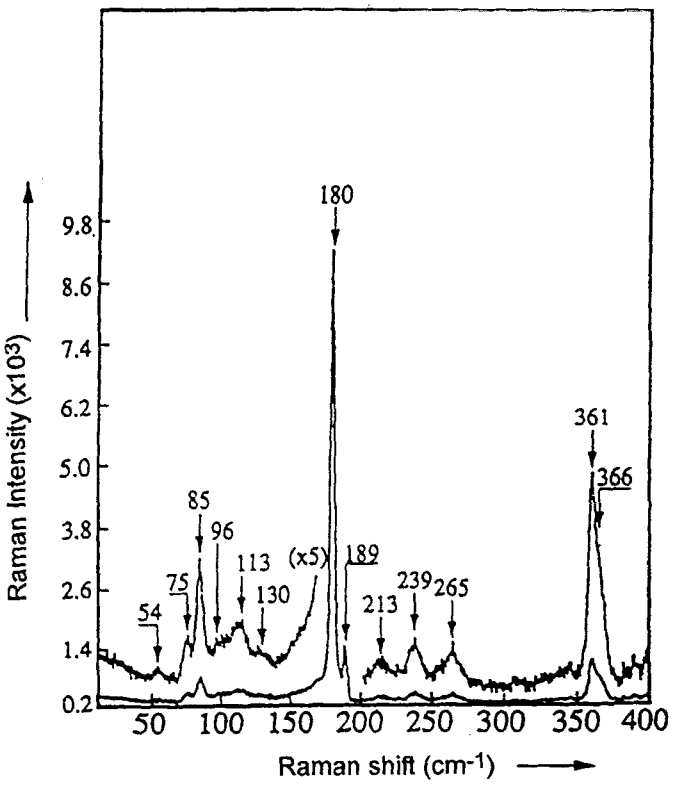

FIGURE 11 Raman spectrum of KI, γ-irradiated at room temperature to 1000 Mrad. The spectrum was measured at 78 K using a laser wavelength of 488 nm with the spectrometer resolution 4 cm^{-1}. Iodine lattice modes are observed at 54, 75, 85, 213, 239 and 265 cm^{-1} (after Comins *et al.* [48]).

experimental information concerning the structures and formation of halogen clusters.

As a further example of Raman spectroscopy in a similar context we consider the recent work of Pariselle *et al.* [49] who have used a Raman microscope to examine the concentrations of I_3^- and I_n^- clusters in RbI bombarded with high energy (13.6MeV/A) argon ions as a function of distance along the ion paths. The results are shown in Figure 12. Comparisons are also made between the experimental results and those of a TRIM-92 calculation, which uses Monte Carlo simulation techniques [50]. There is relatively good agreement between the defect concentrations and the characteristic form of the electronic energy deposition rate which indicates that the excitonic mechanism of defect production is dominant even at very high rates of electronic energy deposition. Indeed, the results strongly

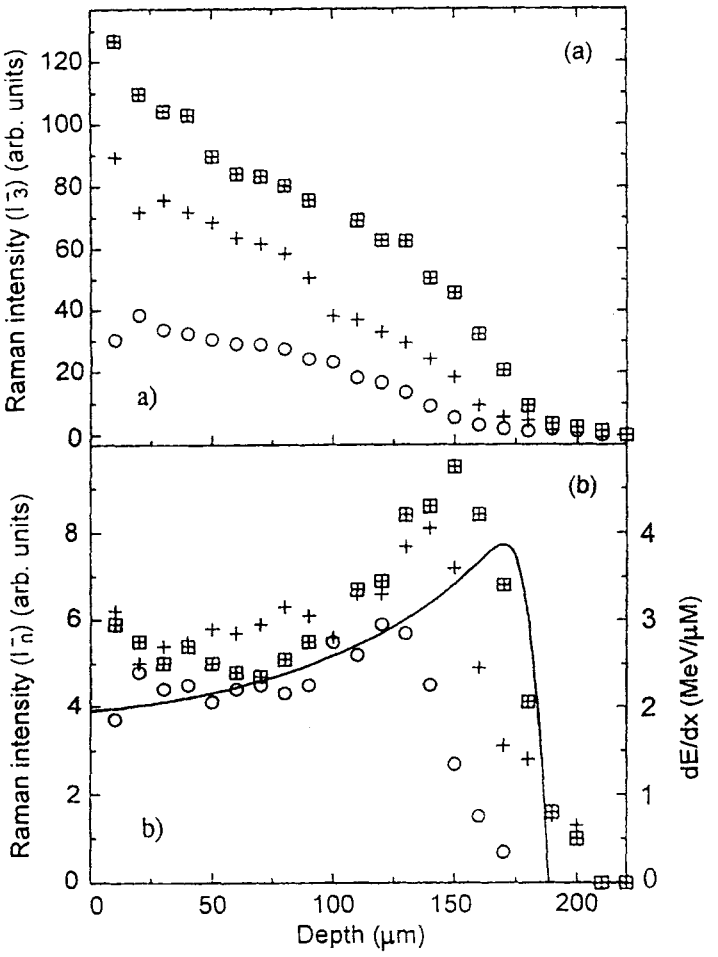

FIGURE 12 (a) Depth profiles of I_3^- clusters at various fluences for RbI bombarded with 13.6 MeV/A argon ions at 300 K. Open circles: for a fluence of 0.5×10^{13} ions/cm^2; squares: for a fluence of 210×10^{13} ions/cm^2. Micro-Raman measurements were conducted at 80 K using laser excitation of wavelength 514.5 nm; (b) Corresponding depth profiles for I_n^- aggregates at the same fluences as in the upper diagram. The same symbols are used for the corresponding fluence values. The solid curve shows the electronic energy deposition profile (Ref. [50]) calculated using TRIM-92 (after Pariselle *et al.* [49]).

suggest the preferential conversion of the smaller I_3^- clusters to the larger I_n^- aggregates in the region where the electronic energy deposition rate is largest. The precise relationship between the I_3^- and I_n^- clusters at a particular depth will depend on their mutually coupled growth kinetics, their dose and dose-rate dependence, the degree of ion-track overlap, and defect

proximity and diffusion effects in cluster formation. Computational simulations would be very useful in the development of a more complete understanding of these complex processes.

SUMMARY

Optical techniques combined with computational simulations provide powerful methods in the study of solids. The work reviewed includes studies of vibrational and/or defect properties of a variety of systems including superionic conductors, opaque solids and thin films, and products of irradiation demage. A better understanding of the experimental results has emerged in many of the cases illustrated by the application of computational simulation techniques; in certain examples, the application of computational modelling to interesting new experimental observations would be very beneficial.

Acknowledgements

The author would like to thank his many collaborators who contributed substantially to the work discussed in detail in this paper; in particular P. E. Ngoepe, P. M. Mjwara, C. R. A. Catlow, A. V. Chadwick, A. G. Every, P. R. Stoddart. W. Pang, X. Zhang, J. C. Crowhurst, A. M. T. Allen, S. Lefrant, E. Rzepka, M. A. Pariselle, E. Balanzat and B. Ramstein.

References

[1] Catlow, C. R. A. (1986). "Computer simulation studies of transport in solids", In: Annual Review of Materials Science, Huggins, R. A., Giordmaine, J. A. and Wachtman, J. B. Jr., Eds., Palo Alto, CA, USA: Annual Reviews, Vol. 16, pp. 517–48.

[2] Hayes, W. (1978). "Superionic conductors", *Contemp. Phys.*, **19**, 469.

[3] "Physics of Superionic Conductors", Topics in Current Physics Series, Salamon, M. B., Ed., Springer, Berlin, 1979.

[4] "Fast Ion Transport in Solids", Vashishta, P., Mundy. J. N. and Shenoy, G. K. Eds., North-Holland, Amsterdam, 1979.

[5] Chadwick, A. V. (1983). " High temperature transport in fluorites", *Solid State Ionics*, **8**, 209.

[6] Catlow, C. R. A., Comins, J. D., Germano, F. A., Harley, R. J. and Hayes, W. (1978). "Brillouin scattering and theoretical studies of high-temperature disorder in fluorite crystals", *J. Phys. C*, **11**, 3197.

[7] Mjwara, P. M., Comins, J. D., Ngoepe, P. E., Bührer, W. and Bill, H. (1991). "Brillouin scattering investigation of the high temperature diffuse phase transition in Li_2S", *J. Phys., Condens. Matter*, **3**, 4289.

[8] Ngoepe, P. E., Comins, J. D. and Every, A. G. (1986). "Brillouin scattering studies of LaF_3 at high temperatures", *Phys. Rev. B*, **34**, 8153.

[9] Ngoepe, P. E., Jordan, W. M., Catlow, C. R. A. and Comins, J. D. (1990). "Computer modelling and Brillouin scattering studies of anharmonicity and high temperature disorder in LaF_3", *Phys. Rev. B*, **41**, 3815.
[10] Ngoepe, P. E. and Comins, J. D. (1988). "Brillouin scattering investigations of cerium fluoride at high temperature: a diffuse superionic transition", *Phys. Rev. Lett.*, **61**, 978.
[11] Mjwara, P. M., Comins, J. D., Ngoepe, P. E. and Chadwick, A. V. (1991). "Brillouin scattering in superionic compounds: NdF_3 and $CaF_2(ReF_2)$", *Radiat. Eff. Defects Solids*, **119–121**, 237.
[12] Comins, J. D., Ngoepe, P. E. and Catlow, C. R. A. (1990). "Brillouin scattering and computer simulation studies of fast ion conductors: a review", *J. Chem. Soc. Faraday Trans.*, **86**, 1183.
[13] Huberman, B. A. (1974). "Co-operative phenomena in solid electrolytes", *Phys. Rev. Lett.*, **32**, 1000.
[14] Rice, M. J., Strassler, S. and Toombs, G. A. (1974). "Superionic conductors: theory of the phase transition to the cation disordered state", *Phys. Rev. Lett.*, **32**, 1596.
[15] Welch, D. O. and Dienes, G. (1977). "Phenomenological and microscopic models of sublattice disorder in ionic crystals, I. Phenomenological models", *J. Phys. Chem. Solids*, **38**, 311.
[16] Catlow, C. R. A. and Mackrodt, W. C. (1982). in Computer Similation of Solids, Catlow, C. R. A. and Mackrodt. W. C., Eds., Lecture Notes in Physics, Vol. 166, Springer, Berlin, Ch. 1.
[17] Lyon, W. G., Osborne, D. W., Flotow, H. E., Grandjean, F., Hubbard, W. N. and Johnson, G. K. (1978). "Thermodynamics of the lanthanide trifluorides. I. The heat capacity of lanthanum trifluoride, LaF_3 from 5 to 350 K and enthalpies from 298 to 1477 K", *J. Chem. Phys.*, **69**, 167.
[18] Jordan, W. M. and Catlow, C. R. A. (1987). "An investigation into the structural and transport properties of LaF_3", *Cryst. Lattice Defects and Amorphous Mater.*, **15**, 81.
[19] Sher, A., Solomon, R., Lee, R. and Muller, M. W. (1966). "Transport properties of LaF_3", *Phys. Rev.*, **144**, 593.
[20] Spedding, F. H., Beaudry, B. J., Henderson, D. C. and Moorman, J. (1974). "High temperature enthalpies and related thermodynamic functions of the trifluorides of Sc, Ce, Sm, Eu, Gd, Tb, Dy, Er, Tm and Yb", *J. Chem. Phys.*, **60**, 1578.
[21] Spedding, F. H. and Henderson, C. D. (1971). "High temperature heat contents and related thermodynamic functions of seven trifluororides of the rare earths: Y, La, Pr, Nd, Gd, Ho and Lu", *J. Chem. Phys.*, **54**, 2476.
[22] Nizzoli, F. and Sandercock, J. R. (1990) "Surface Brillouin scattering from phonons", In: Dynamical Properties of Solids, Vol. 6; The Modern Physics of Phonons: Transport, Surfaces and Simulations, Horton, G. K. and Maradudin, A. A., Eds., North Holland, Amsterdam, Ch. 5, 281–335.
[23] Hillebrands, B., Baumgart, P., Mock, R., Güntherodt, G. and Bechthold, P. S. (1985). "Dispersion of localized elastic modes in thin supported gold layers measured by Brillouin scattering", *J. Appl. Phys.*, **58**, 3166.
[24] Mendik, M., Satish, S., Kulik, A., Gremaud, G. and Wachter, P. (1992). "Surface acoustic wave studies on single crystal nickel using Brillouin scattering and scanning acoustic microscopy", *J. Appl. Phys.*, **71**, 2830.
[25] Mutti, P., Bottani, C. E., Ghislotti, G., Beghi, M., Briggs, G. A. D. and Sandercock, J. R. (1995). "Surface Brillouin scattering - extending surface wave measurements to 20 GHz", In: Advances in Acoustic Microscopy, Vol. 1, Andrew Briggs, Ed., Plenum Press, New York, Ch. 7, 249–300.
[26] Loudon, R. (1978)."Theory of surface-ripple Brillouin scattering by solids", *Phys. Rev. Lett.*, **40**, 581.
[27] Bortolani, V., Nizzoli, F. and Santoro, G. (1978). "Surface density of acoustic phonons in GaAs", *Phys. Rev. Lett.*, **41**, 39.
[28] Every, A. G., Kim, K. Y. and Maznev, A. A. (1997). "The elastodynamic response of a semi-infinite anisotropic solid to sudden surface loading", *J. Acoust. Soc. Am.*, **102**, 1346.
[29] Farnell, G. W. and Adler, E. L. (1972). "Elastic wave propagation in thin layers", In: Physical Acoustics, Mason, W. P. and Thurston, R. N., Eds., Academic Press, New York, Vol. 6, 35–127.

[30] Stoddart, P. R., Comins, J. D. and Every, A. G. (1995). "Brillouin scattering measurements of surface acoustic wave velocities in silicon at high temperatures", *Phys. Rev. B*, **51**, 17574.
[31] Stoddart, P. R., Comins, J. D. and Every, A. G. (1996). "High-temperature studies of surface acoustic wave velocities in silicon by Brillouin scattering", *Physica B*, **219 and 220**, 717.
[32] Pang, W., Stoddart, P. R., Comins, J. D., Every, A. G., Pietersen, D. and Marais, P. J. (1997). "Elastic properties of TiN hard films at room and high temperatures using Brillouin scattering", *Int. J. Refract. Met. Hard Mater.*, **15**, 179.
[33] Every, A. G., Pang, W., Comins, J. D. and Stoddart, P. R. (1997). "Brillouin scattering study of guided modes in TiN films on high speed steel", *Ultrasonics*, **36**, 223.
[34] Lefrant, S. and Rzepka, E. (1979). "Raman study of V-centres in X-irradiated KI", *J. Phys. C*, **12**, L573.
[35] Lefrant, S. and Rzepka, E. (1980). "Raman study of V-centres in X-irradiated KI and RbI", *I. Phys. Colloq.*, **41**, C6–476.
[36] Taurel, L., Rzepka, E. and Lefrant, S. (1983). "Raman scattering induced by V centres and their aggregates in alkali halides", *Radiat. Eff.*, **72**, 115.
[37] Rzepka, E., Lefrant, S., Taurel, L. and Hughes, A. E. (1981). "Raman scattering induced by V-centre aggregates in pure and Ca-doped KI X-irradiated at room temperature", *J. Phys. C*, **4**, L767.
[38] Allen, A. M. T., Comins, J. D. and Ford, P. J. (1985). "A Raman study of defect annealing in gamma-irradiated KI", *J. Phys. C*, **18**, 5783.
[39] Allen, A. M. T. and Comins, J. D. (1987)."Optical studies of KI gamma-irradiated at room temperature and annealed to high temperature", *Cryst. Lattice Defects and Amorphous Mater.*, **17**, 93.
[40] Rzepka, E., Bernard, M., Lefrant, S. and Comins, J. D. (1987). "Spectroscopic characteristic of bromine aggregates in KBr crystals", *Cryst. Lattice Defects and Amorphous Mater.*, **17**, 113.
[41] Allen, A. M. T. and Comins, J. D. (1992). "Halogen defect aggregation in KI irradiated between 195 K and 295 K", *Nucl. Instrum. Methods Phys. Res. B, Beam Interact. Mater. At.*, **65**, 516.
[42] Allen, A. M. T. and comins, J. D. (1992). "Raman study of H-centre aggregation in γ-irradiated RbI: evidence for I_3^- and I_2^0 di-interstitial defects", *J. Phys., Condens. Matter*, **4**, 2701.
[43] Williams, R. T. and Song, K. S. (1990). "The self-trapped exciton", *J. Phys. Chem. Solids*, **51**, 679.
[44] Itoh, N. and Tanimura, K. (1990). "Formation of interstitial-vacancy pairs by electronic excitation in pure ionic crystals", *J. Phys. Chem. Solids*, **51**, 717.
[45] Dienes, G. J., Hatcher, R. D. and Smoluchowski, R. (1970). "Formation and structure of H Centres", *J. Phys. Chem. Solids*, **31**, 701.
[46] Catlow, C. R. A., Diller, K. M. and Hobbs, L. W. (1980). "Irradiation-induced defects in alkali halide crystals", *Philos. Mag. A*, **42**, 123.
[47] Hobbs, L. W., Hughes, A. E. and Pooley, D. (1973). "A sutdy of interstitial clusters in irradiated alkali halides using direct electron microscopy", *Proc. R. Soc. London Ser. A*, **332**, 167.
[48] Comins, J. D., Allen, A. M. T., Rzepka, E. and Lefrant, S. (1995). "Raman and optical absorption studies of the annealing of γ-irradiated KI and KI(Sr)", *Radiat. Eff. Defects Solids*, **136**, 295.
[49] Pariselle, M. A., Lefrant, S., Balanzat, E., Ramstein, B. and Comins, J. D. (1996). "Depth profiles of interstitial halogen defects in high-energy ion-bombarded RbI by micro-Raman spectroscopy", *Phys. Rev. B*, **53**, 11365.
[50] Ziegler, J. S., Biersack, J. P. and Littmark, V. (1995). "The Stopping and Range of Ions in Solids", Pergamon, Oxford.